Energy xxx (2014) 1–10

Contents lists available at ScienceDirect

Energy

journal homepage: www.elsevier.com/locate/energy

Energy production from tidal currents in an estuary: A comparative study of floating and bottom-fixed turbines

M. Sánchez [a, *], R. Carballo [a], V. Ramos [a], G. Iglesias [b]

[a] University of Santiago de Compostela, Hydraulic Engineering, Campus Univ. s/n, 27002 Lugo, Spain
[b] University of Plymouth, School of Marine Science and Engineering, Marine Building, Drakes Circus, Plymouth PL4 8AA, United Kingdom

ARTICLE INFO

Article history:
Received 12 June 2014
Received in revised form
18 September 2014
Accepted 20 September 2014
Available online xxx

Keywords:
Tidal stream energy
Tidal turbine
Ria de Ortigueira
Estuary
Numerical modelling

ABSTRACT

In a tidal stream project the selection of the most appropriate device is of major importance. The aim of this work is to investigate the difference between two tidal farms, one with floating TSTs (Tidal Stream Turbines), the other with bottom-fixed TSTs, in terms of annual performance and its monthly variability. This investigation is carried out considering real operational conditions in a case study: Ria de Ortigueira (NW Spain), a drowned river valleys which is one of the most promising sites for tidal stream energy exploitation in the Iberian Peninsula. A 3D, high-resolution, numerical model is applied to simulate the hydrodynamics of the ria during an entire year with either the floating or bottom-fixed TSTs, and, on these grounds, determine the most representative performance parameters. Significant differences emerge in the performance of both plants; these are due to a great extent to the vertical variation in the flow velocity, which is relevant at many sites of interest for tidal stream energy exploitation such as Ria de Ortigueira. Finally, relevant variations were identified in the intra-annual performance which must be borne in mind in dimensioning the plant.

1. Introduction

In the late 90's social pressure emerged claiming for a new, sustainable energy production and utilisation model [1]. This, together with a number of policies aimed at curbing greenhouse gas emissions and the realisation that the current energy model, with fossil fuels at its core, is necessarily limited in time, has resulted in companies and governments around the world being currently working intensively on the development and efficient utilisation of new and renewable energy sources [2].

Tidal stream energy is one of the most attractive and promising renewable energy sources owing to its advantages relative to other renewables: no land occupation, a high load factor (water density is ~800 times higher than air density), flow predictability and consequently power production predictability, inexistence of extreme flows (which might otherwise damage the conversion devices), etc. are some of the advantages of tidal stream energy exploitation [3–6]. However, due to the relatively recent interest in this type of energy (in comparison with other renewables such as wind or solar energy), only a few TECs (Tidal Energy Converters) have achieved at this point a commercial or pre-commercial stage [7,8]. The conversion principle varies between the different TECs developed or in a development stage. Generally speaking, there exist two types of TECs, based on either the reciprocating or rotating principle. The latter, also known as TSTs (Tidal Stream Turbines), is the most popular. TSTs can be: (i) floating beneath the surface and anchored to the bottom by means of chains or cables (floating TSTs), or (ii) rigidly attached to the bottom by means of a structure (bottom-fixed TSTs) [9,10]. As a result of their different configuration, despite them being installed at the same coastal site, their performance may differ due to the varying hydrodynamic conditions throughout the water column (each type of TST is located at a different position within the water column). However, the implications for the power performance of opting for either floating or bottom-fixed devices have not been investigated as far as the authors are aware.

The aim of this study is to examine the differences in the power performance in real conditions of operation of two tidal stream plants, composed by either floating or bottom-fixed TSTs, proposed in a previous work [11], where their impacts on the estuarine hydrodynamics were analysed. For this purpose, a 3D high-resolution numerical model is implemented in the Ria de Ortigueira, a drowned river valleys which is a promising site for tidal stream energy exploitation located in Galicia (NW Spain) (Fig. 1). On the basis of the numerical results a detailed intra-annual power performance assessment of floating and bottom-fixed tidal plants have

* Corresponding author. Tel.: +34 982823650; fax: +34 982285926.
E-mail address: marcos.sanchez@usc.es (M. Sánchez).

http://dx.doi.org/10.1016/j.energy.2014.09.053
0360-5442/

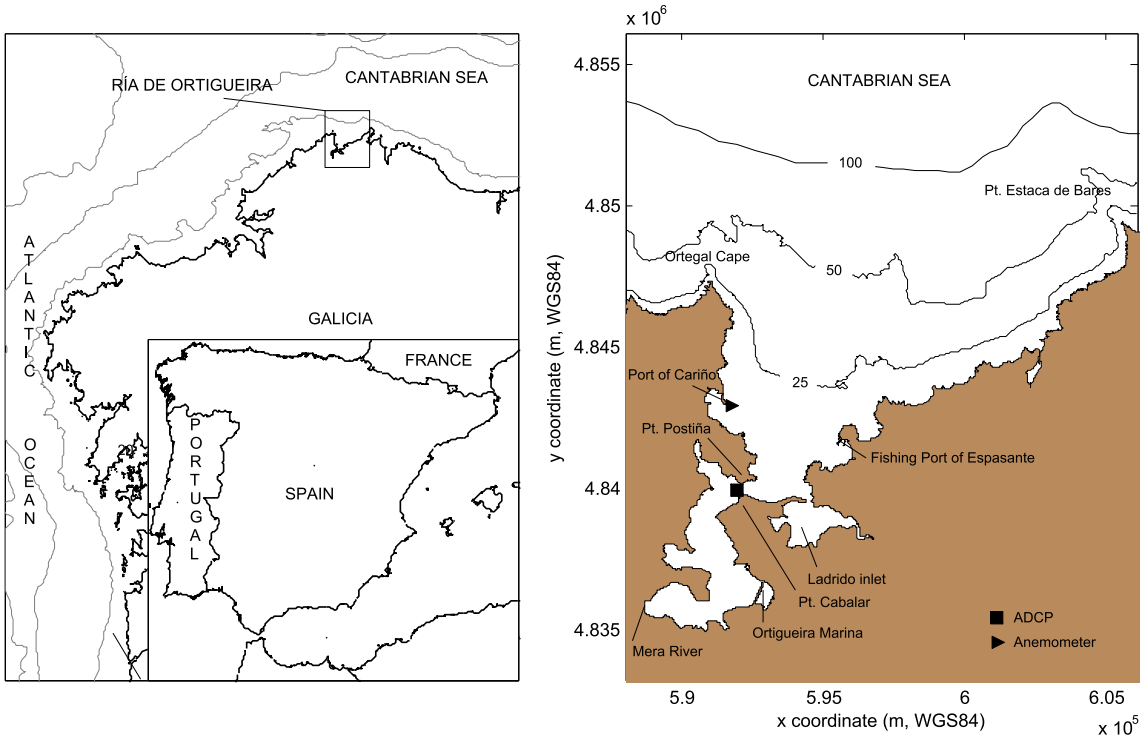

Fig. 1. Situation of Ria de Ortigueira in the Iberian Peninsula (left-hand side plots) and detailed view of the ria (right-hand side plot).

been conducted so as to investigate the importance of selecting the type of TST that performs best considering the specific hydrodynamic conditions of the area of interest.

2. Methodology

2.1. Three-dimensional hydrodynamics model

The 3D hydrodynamics model Delft3D-FLOW was used to compute the flow conditions in Ria de Ortigueira in the presence of a tidal stream farm. This model has been widely used to investigate coastal hydrodynamics in semi-enclosed water bodies [5,12–19]. Given that the Galician Rias usually present a stratified flow pattern (e.g. [20–22], to properly analyse the ria's hydrodynamics, and as a result to conduct reliable energy computations, in this work a 3D model was implemented.

Delft3D-FLOW is a finite-difference code that solves the three-dimensional Navier–Stokes equations for incompressible free surface flow coupled to the transport equation [23]. In this manner baroclinic effects, which can be of great importance in the case of rias or estuaries [24], can be taken into account. The model equations are as follows:

$$\frac{\partial u}{\partial x}+\frac{\partial v}{\partial y}+\frac{\partial w}{\partial z}=Q, \tag{1}$$

$$\left.\begin{aligned}\frac{Du}{Dt}&=fv-g\frac{\partial \zeta}{\partial x}-\frac{g}{\rho_0}\int_{z'=z}^{z'=\zeta}\frac{\partial \rho}{\partial x}dz'+\upsilon_h\left(\frac{\partial^2 u}{\partial x^2}+\frac{\partial^2 u}{\partial y^2}\right)+\upsilon_v\left(\frac{\partial^2 u}{\partial z^2}\right)\\ \frac{Dv}{Dt}&=-fu-g\frac{\partial \zeta}{\partial y}-\frac{g}{\rho_0}\int_{z'=z}^{z'=\zeta}\frac{\partial \rho}{\partial y}dz'+\upsilon_h\left(\frac{\partial^2 v}{\partial x^2}+\frac{\partial^2 v}{\partial y^2}\right)+\upsilon_v\left(\frac{\partial^2 v}{\partial z^2}\right)\end{aligned}\right\}, \tag{2}$$

$$\frac{\partial p}{\partial z}=-\rho g, \tag{3}$$

$$\frac{Dc}{Dt}=D_h\left(\frac{\partial^2 c}{\partial x^2}+\frac{\partial^2 c}{\partial y^2}\right)+D_v\frac{\partial^2 c}{\partial z^2}-\lambda_d c+R_s. \tag{4}$$

Equation (1) represents the conservation of mass under the assumption of incompressibility; Equation (2) represents the conservation of momentum in the x- and y-directions; Equation (3) expresses the conservation of momentum in the vertical direction which under the shallow-water assumption simplifies to the hydrostatic pressure distribution; finally, Equation (4) is the transport equation, which is solved in the present study for both salinity and temperature. In these equations, x, y and z represent the east, north and vertical directions, respectively and u, v and w the velocity components in the aforementioned directions; ζ is the free surface elevation above the datum; Q represents the intensity of mass sources per unit area; f is the Coriolis parameter; g is the gravitational acceleration, υ_h and υ_v are the horizontal and vertical eddy viscosity coefficients respectively, and ρ and ρ_0 are the density and the reference density of sea water, respectively. Finally, in the transport equation, c stands for salinity or temperature; D_h and D_v are the horizontal and vertical eddy diffusivity coefficients, respectively; λ_d represents the first order decay process; and R_s is the source term.

2.2. TSTs modelling

The flow conditions within a ria change as a result of the operation of the TSTs and the energy that they extract from the flow. If the flow at the locations of the TSTs and, consequently, their yield are to be accurately determined, it is therefore necessary to take them into account in the model. The operation of a turbine can be simulated by considering its effect on the flow, i.e., by adding a retarding force with the same magnitude as that exerted by the

Please cite this article in press as: Sánchez M, et al., Energy production from tidal currents in an estuary: A comparative study of floating and bottom-fixed turbines, Energy (2014), http://dx.doi.org/10.1016/j.energy.2014.09.053

flow on the turbine but opposite direction. The common procedure for modelling this force is as a momentum sink [18,21,25–27]. On this basis, in this study the retarding force was introduced into the model by adding the following sink terms to the right-hand side of the momentum equations (Equation (2)) in the x- and y-directions:

$$\left.\begin{aligned} M_x &= -\frac{1}{2}\frac{C_T A}{V}Uu \\ M_y &= -\frac{1}{2}\frac{C_T A}{V}Uv \end{aligned}\right\}, \tag{5}$$

where M_x and M_y represent the momentum of the external forces per unit volume, V_c, in the x- and y-directions, respectively; U is the component of the effective flow velocity perpendicular to the turbine; A_t is the cross-sectional area of the turbine rotor; and C_T is the thrust coefficient (an aerodynamic coefficient given by the lift and drag coefficients) which is related to the power coefficient, C_p [28].The floating and bottom-fixed TSTs are modelled by introducing the retarding force in the vertical layers of the model corresponding to the water depth at which they operate.

2.3. Performance analysis

The analysis of the performance of a tidal stream farm can be based on three characteristic parameters describing the operation of the individual TSTs in the farm [29]: electrical energy output, capacity factor and availability factor. The electrical energy output of the i-th TST of a tidal farm over the period from $t = 0$ to $t = t_1$ is given by

$$E_e^i = \int_0^{t_1} P_e(t)\,\mathrm{d}t, \tag{6}$$

where $P_e(t)$ is the electrical power output of the TST, which can be expressed as [30]

$$P_e(t) = \frac{1}{2}C_p(v)\rho A_t[U(t)]^3, \tag{7}$$

where $C_p(v)$ is the power coefficient, defined as the ratio between the power available from the flow and the electrical power output. Its value varies with the flow velocity in a manner that is specific of each TST.

Table 1
Main technical specifications of the Evopod turbine [D, rotor diameter; V_{ci}, cut-in velocity; V_r, rated velocity; V_{co}, cut-off velocity; P_r, rated power; A, swept area; C_{pNO}, power coefficient in normal operation; C_{pSC}, power coefficient in stall control].

D (m)	5
V_{ci} (ms^1)	0.7
V_r (ms^1)	2.2
V_{co} (ms^1)	3.1
A (m^2)	19.6
Pr (kW)	40
C_{pNO}	0.35
C_{pSC}	0.2

Therefore, the electrical energy output of the entire tidal farm is

$$E_e = \sum_{i=1}^{n} E_e^i, \tag{8}$$

where n is the number of TSTs of the farm.

The availability factor (A_f) is the ratio between the time during which the TST is actually generating power (T_g) – TSTs have a minimum (*cut-in*) and a maximum (*cut-off*) flow velocity, below and above which they do not generate electricity – and the total duration of the period considered (T_a):

$$A_f = \frac{T_g}{T_a}. \tag{9}$$

The capacity factor (C_f) represents the ratio between the electrical energy output over a period of interest (E_e) and the electrical energy output the TST would have produced over the same period had it operated at rated power ($P_r T_a$):

$$C_f = \frac{E_e}{T_a P_r}. \tag{10}$$

The information contained in the capacity factor can be expressed in terms of an annual cycle by means of the equivalent full-load hours:

$$FLH = \frac{E_e^a}{P_r}, \tag{11}$$

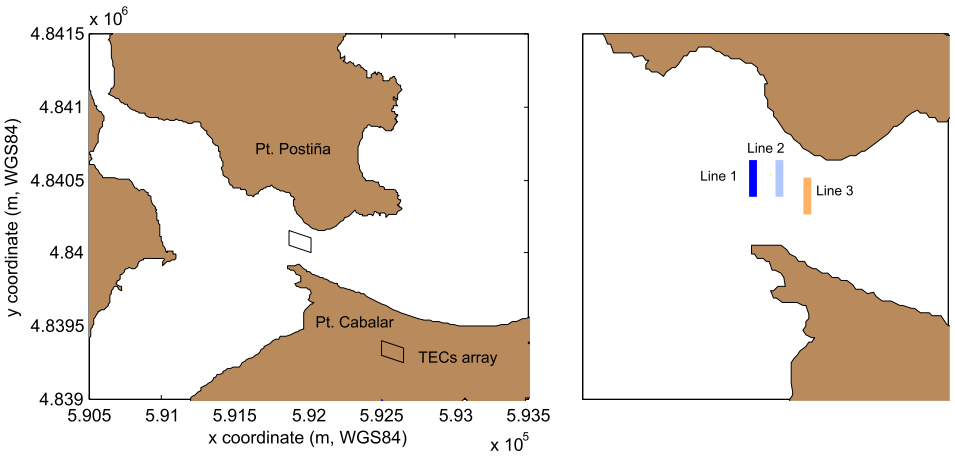

Fig. 2. Area occupied by the proposed tidal stream plants (left-hand side plot) and their layout (right-hand side plot).

Please cite this article in press as: Sánchez M, et al., Energy production from tidal currents in an estuary: A comparative study of floating and bottom-fixed turbines, Energy (2014), http://dx.doi.org/10.1016/j.energy.2014.09.053

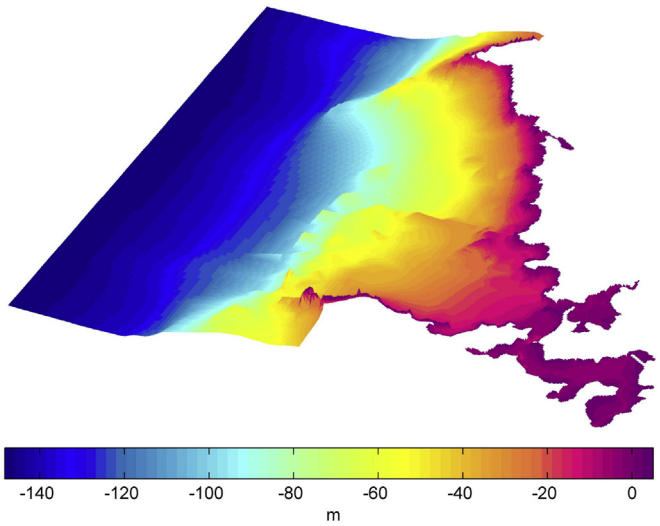

Fig. 3. Three-dimensional representation of the bathymetry of Ria de Ortigueira.

where E_e^a is the annual electric energy output. The equivalent full-load hours represent the number of hours a turbine would have to operate at its rated power to produce the same amount of energy that it actually produced over a year.

To determine these parameters it is necessary, first, to define the location and characteristics of the tidal stream farm and, second, to implement a numerical model of the hydrodynamics in the area that taking into account the energy extracted by the farm. The implementation of the numerical model enables to obtain the perturbed flow velocities, which in turn are necessary for the computation of the aforementioned parameters.

3. Application to Ria de Ortigueira

3.1. Study site and proposed tidal plants

The rugged coastline of NW Spain is characterised by the rias, a specific type of primary estuary developed in high relief coasts drowned by the rise of sea level during Holocene [31–33], regarded as promising sites for tidal stream energy exploitation. These rias can be roughly divided into Rias Altas, or Higher Rias, Rias Centrales or Central Rias, and Rias Baixas or Lower Rías [14,34]. Owing to its complex geomorphology characteristics and its high tidal range, the Ria de Ortigueira (Fig. 1), one of the Rias Altas, is amongst the most promising sites for tidal stream energy exploitation in the Iberian Pensinsula [15,35].

Ria de Ortigueira is delimited by Cape Ortegal and Pt. Estaca de Bares (Fig. 1). With an approximate area of 85 km and a length along its main axis of approx. 18 km, it is, by far, the largest of the Rias Altas. The tidal flow is strongest at two constrictions in its inner part where the highest current velocities occur. One of them is located to the East, between the main lobe of the ria and the Ladrido Inlet, and the other is located to the West, in the channel between Pt. Postiña and Pt. Cabalar. By applying the TSE (Tidal Stream Exploitability) index to this ria [15] the optimum site for the installation of a tidal stream farm was selected as follows. According to the TSE index values obtained, the former (eastern) constriction has a TSE of 0 owing to its insufficient water depth, and therefore it is considered inappropriate for tidal stream energy exploitation. By contrast, the TSE index value of the latter (western) constriction exceeds 5 – the largest value over the entire ria. Therefore, this area combines a substantial resource with an appropriate depth, implying that it is an appropriate site for an array of TSTs in Ria de Ortigueira (Fig. 2).

Two tidal stream farms were considered in this study, both composed of 30 turbines distributed in three lines roughly perpendicular to the main flow direction. The TST selected for the plants was an Evopod turbine [36] in view of its appropriateness for shallow waters areas (Table 1). The surface occupied in plan view by each farm is about 1500 m^2, corresponding to a sweep area of approx. 600 m^2. Both arrays proposed are located at the same site and present the same layout (Fig. 2) but differ in their vertical configuration. The first plant (P1) is composed of floating TSTs [36] occupying roughly the upper 65 per cent of the water column; the second plant (P2) is composed by TSTs with exactly the same mechanical characteristics, but fixed to the bottom, occupying approximately the lower 65 per cent of the water column.

Table 2
Main tidal constituents in the Ria de Ortigueira.

Constituent	Amplitude (cm)	Phase (°)
M2	122.79	90.15
S2	42.91	121.08
N2	25.98	70.39
K2	12.03	118.76
K1	7.35	73.49
O1	6.22	324.62
P1	2.22	65.15
Q1	2.11	271.31
M4	1.45	334.80

Table 3
Value of Manning's coefficient function of water depth.

H	n
$-2.5 \le H < -2.0$	0.042
$-2.0 \le H < -1.5$	0.038
$-1.5 \le H < 1.0$	0.034
$-1.0 \le H < -0.5$	0.030
$-0.5 \le H < 0.0$	0.027
$0.0 \le H < 0.5$	0.024
$0.5 \le H < 1.0$	0.022
$1.0 \le H < 3.0$	0.020
$3 \le H < 10$	0.018
$10 < H$	0.015

3.2. Model implementation

The numerical model previously described in Sections 2.1 and 2.2 was implemented in Ria de Ortigueira. For this purpose a Cartesian, varying-size numerical grid, with a total of 57361 cells was created covering the whole ria and extending up to the 150 m isobath. The grid size was finer (50 × 50 m) in the inner and middle ria than in the outer ria and on the shelf, where it decreased in the y-direction up to values of 50 × 150 m at the northern outer boundary. As regards the vertical grid discretisation, a σ-coordinate

Table 4
Correlation coefficient between computed and measured time series of sea level (R_ζ) and flow velocity magnitude and direction (R_M and R_D respectively).

Water level		Current velocity			
			Surface layer	Middle layer	Bottom layer
R_ζ	0.9895	R_M	0.8965	0.8619	0.8439
		R_D	0.8509	0.8375	0.8215

Please cite this article in press as: Sánchez M, et al., Energy production from tidal currents in an estuary: A comparative study of floating and bottom-fixed turbines, Energy (2014), http://dx.doi.org/10.1016/j.energy.2014.09.053

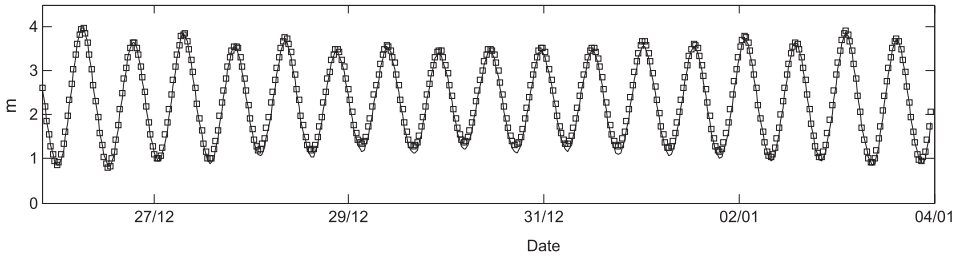

Fig. 4. Comparison between computed (–) and measured (□) water levels in the ADCP location during the validation period.

system [37] with twelve layers was used. The layer thickness (% of water column) from surface to bottom was, as a percentage of the water column: 2, 3, 5, 10, 15, 15, 15, 15, 10, 5, 3 and 2. The resolution of the grid is higher near the seabed and surface in order to better resolve boundary layers flow. To close the turbulence the k-ε model [38] was adopted. Finally, the bathymetry (Fig. 3) was obtained from nautical charts 408 and 4083 from the Hydrographic Institute of the Spanish Navy (*Instituto Hidrografico de la Marina*) and interpolated onto the computational grid.

With regard to the boundary conditions, Dirichlet conditions were imposed along the open boundary by prescribing the sea surface level based on the main tidal harmonics (Table 2) together with daily thermohaline conditions. At the land margins the forcings were null flow through the boundary and zero shear stress (free slip). On the other hand, the shear stress at the seabed, τ_{b3D}, induced by a turbulent flow is related to the current velocity above the bed:

$$\vec{\tau}_{b3D} = \frac{\rho_0 g \vec{u}_b |\vec{u}_b|}{C_{3D}^2}, \tag{12}$$

where $\vec{u}_b$ is the magnitude of the horizontal velocity in the lowest layer (immediately above the bed) and C_{3D} is the 3D Chézy coefficient, given by

$$C_{3D} = C_{2D} + \frac{\sqrt{g}}{\kappa} \ln\left(\frac{\Delta z_b}{2H}\right), \tag{13}$$

with κ the von Karman constant ($\kappa = 0.41$), Δz_b the vertical distance from the seabed to the nearest computational grid point, H the total water depth and C_{2D} the 2D Chézy coefficient, which can be determined based on Manning's coefficient, n, as follows:

$$C_{2D} = \frac{\sqrt[6]{H}}{n}. \tag{14}$$

Manning's coefficient is assumed to be depth-dependent according to previous studies [13,39–41]; the value considered for each water depth range is shown in Table 3.

Finally, at the free surface the wind shear-stress, τ_s, is defined as

$$\vec{\tau}_s = \rho_a C_d U_{10}^2 \tag{15}$$

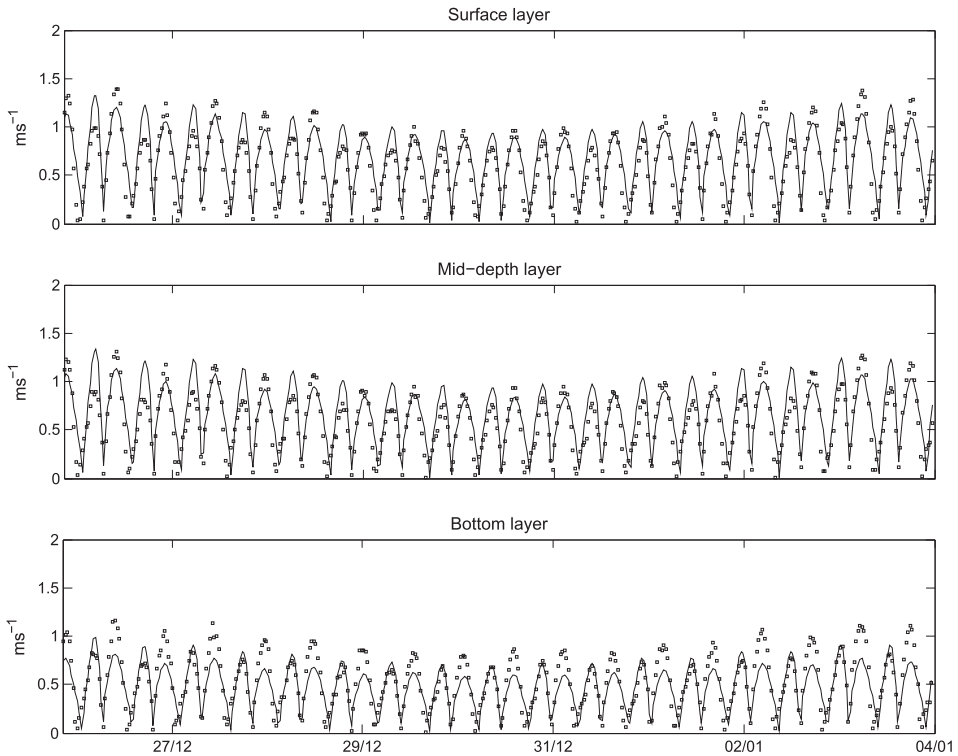

Fig. 5. Comparison between computed (–) and measured (□) current speed for the surface, mid-depth and bottom layers in the ADCP location during the validation period.

Please cite this article in press as: Sánchez M, et al., Energy production from tidal currents in an estuary: A comparative study of floating and bottom-fixed turbines, Energy (2014), http://dx.doi.org/10.1016/j.energy.2014.09.053

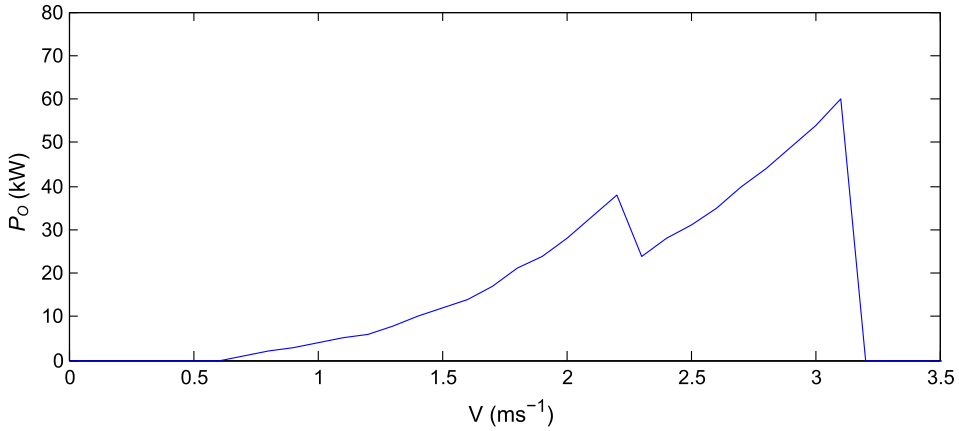

Fig. 6. Power curve of the Evopod turbine [V, flow velocity; P_O, electrical power output].

where ρ_a is the density of the air, U_{10} the wind speed at 10 m above the sea surface and C_d the wind drag coefficient, calculated following [42] and [43].

The tidal stream plant was implemented in the model by using the momentum sink approach as described in Section 2.2. In the case of P1 and P2, the retarding force affects the 7 upper or lower layers of the model, respectively. In both cases the value of C_T considered is 0.8, which corresponds to a value of the power coefficient, C_p, of 0.35 [28].

3.3. Model validation

The numerical model was validated by comparing the numerical results with field data of water level and current velocity. For this purpose, an ADCP (Acoustic Doppler Current Profiler) Sontek Argonaut XR and two CTD (Conductivity Temperature a Depth) sensors Seabird Microcat 37 were deployed in Ria de Ortigueira (Fig. 1) over a 19-day period. During the validation period, the numerical model was forced with the main tidal harmonics (Table 2) and daily conditions of salinity and temperature at the open boundaries, wind data every thirty minutes, and daily fluvial discharge data.

The correlation coefficients between measured and computed time series of water level and current velocity direction and magnitude were computed (Table 4). It can be observed that the resulting correlation coefficients are close to the unit for both variables. The excellent agreement between measured and computed water level can be observed in Fig. 4 over 9-day time series representation. In the same way the excellent agreement between time series of numerical and measured velocities can be observed in Fig. 5 at three points of the water column: surface, mid-depth and bottom.

Table 5
Annual parametric analyse of the different lines of the array.

		Floating TSTs (P1)	Bottom-fixed TSTs (P2)
E_e (MWh)	Line 1	1.161×10^3	0.684×10^3
	Line 2	0.673×10^3	0.426×10^3
	Line 3	0.591×10^3	0.389×10^3
	Array	2.425×10^3	1.498×10^3
A_f	Line 1	0.63	0.53
	Line 2	0.53	0.41
	Line 3	0.50	0.39
	Array	0.63	0.53
C_f	Line 1	0.33	0.19
	Line 2	0.19	0.12
	Line 3	0.17	0.11
	Array	0.23	0.14
FLH	Line 1	2902	1710
	Line 2	1682	1065
	Line 3	1479	971
	Array	2021	1249

4. Power performance analysis

Two long-term numerical simulations covering an entire year (Case 1 and Case 2, each of them considering a different tidal farm) were performed. In Case 1, the array introduced in the model is composed of floating TSTs (Plant P1), and in Case 2, of bottom-fixed TSTs (Plant P2). Next, on the basis of the numerical simulations and the characteristics of the turbine selected (Table 1 & Fig. 6), the power performance throughout the entire year of the two tidal farms proposed was computed according to the parameters previously defined (Section 2.3).

The forcing factors considered were the main tidal harmonics (Table 2), monthly averaged salinity and temperature conditions along the open boundary and monthly averaged river discharge. The velocity considered for electrical power generation is the velocity at rotor height, as in the case of wind generators, which varies depending on the case study (1 or 2) as a result of the different water depth at which the rotor is located.

The differences in the power performance of the two plants analysed are significant (Table 5). The annual energy production of P1 is 2.425×10^3 MWh, whereas the production of P2 is around 40% less. These differences are even larger in the case of the first row of TSTs (hereafter referred to as Line 1), whose energy production is almost double in the case of floating TSTs (P1) relative to bottom-fixed units (P2). These results prove that in a coastal area with significant differences in the flow speed throughout the water column, such as the study area, significant differences can arise between the power performance of plants composed of floating or bottom-fixed TSTs.

As a regard the operation time, the values of the availability factor (A_f) show that P1 and P2 operate during 63% and 48% of the time, respectively. This would have implications if an energy storage system was required – it would have to be substantially larger for P2 given its lower operation time. Regarding the capacity factor (C_f), the differences are even higher, roughly 64% (0.23 and 0.64 for P1 and P2, respectively), indicating an important advantage of P1, for a higher capacity factor is associated with a better production to capital investment ratio. These important differences are directly

Please cite this article in press as: Sánchez M, et al., Energy production from tidal currents in an estuary: A comparative study of floating and bottom-fixed turbines, Energy (2014), http://dx.doi.org/10.1016/j.energy.2014.09.053

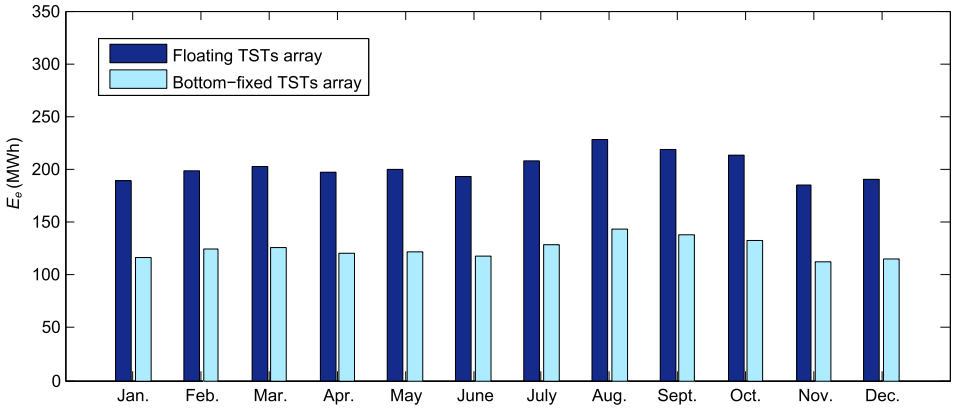

Fig. 7. Monthly electrical energy output [E_e] of floating and bottom-fixed tidal plants.

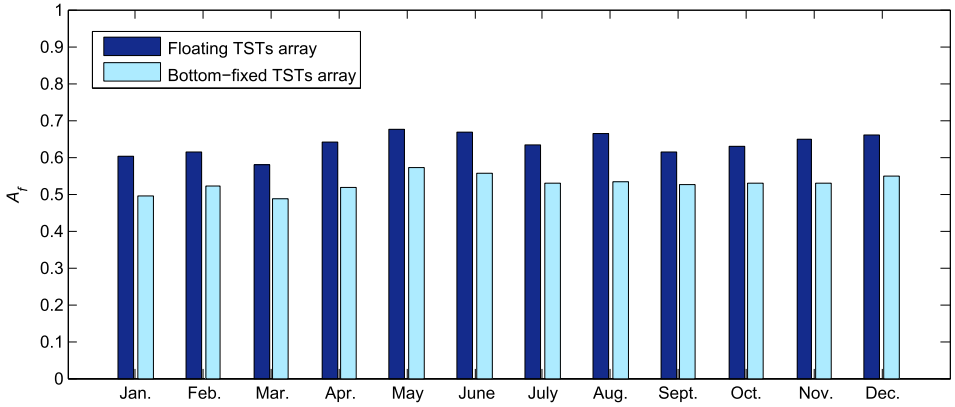

Fig. 8. Monthly availability factor [A_f] of floating and bottom-fixed tidal plants.

transferred to the equivalent *FLH* (full-load hours): P1 has over 2000 *FLH*, and P2 only about 1250 *FLH*. Although a detailed study of the installation costs would be necessary for an exhaustive analysis of the profitability of the proposed plant, the low *FLH* of P2 does not contribute to its economic viability.

On the basis of the numerical simulations and the characteristics of the turbine selected, the monthly power performance parameters defined in section 2.3 were determined for P1 and P2 (Figs. 7–9). The intra-annual power performance presents a significant variability, which should be analysed to ascertain the optimum tidal farm configuration. In the case of the energy production (Fig. 7), the month with highest E_e is August (227.74 MWh and 143.44 MWh for P1 and P2, respectively); on the other hand, November presents the lowest E_e (185.52 MWh for P1 and 112.76 for P2, about 20% lower than that of August).

An important aspect that should be noted is that, far from what might be expected, it is not in the months with the largest tides, and therefore the strongest velocity peaks, that the energy production is largest – or, more generally, that the farm performance is best. The explanation lies in that in the months with highest tides (March and September) there exist important differences between tidal cycles (with peak velocities ranging from 2.2 ms−1 to

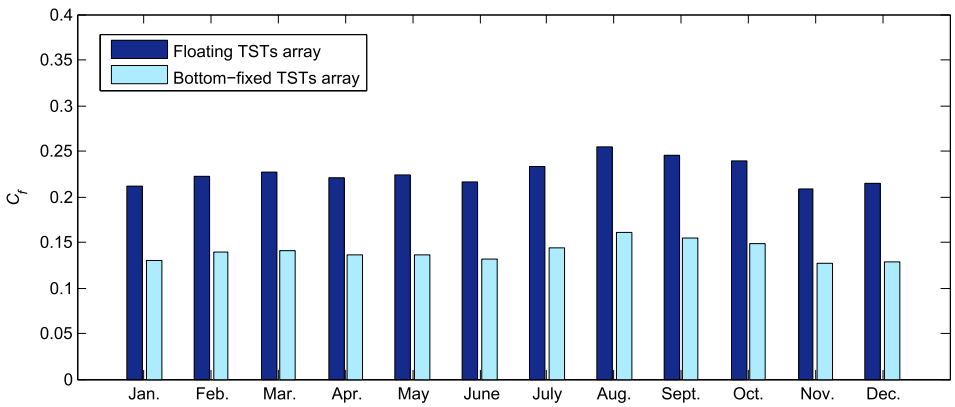

Fig. 9. Monthly capacity factor [C_f] of floating and bottom-fixed tidal plants.

Please cite this article in press as: Sánchez M, et al., Energy production from tidal currents in an estuary: A comparative study of floating and bottom-fixed turbines, Energy (2014), http://dx.doi.org/10.1016/j.energy.2014.09.053

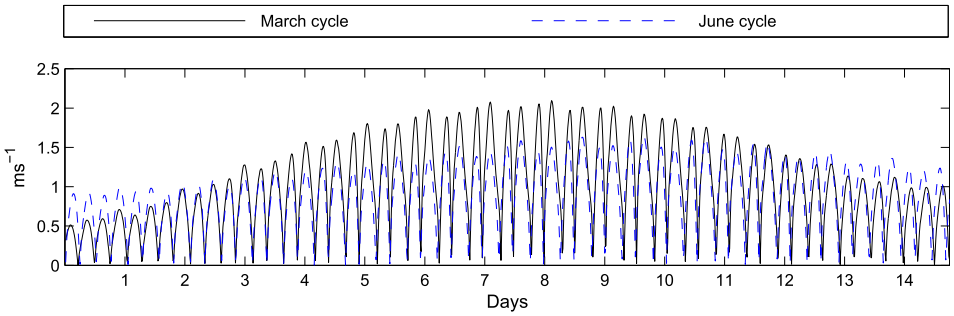

Fig. 10. Comparison between flow velocities throughout two spring-neap cycles during March and June.

0.5 ms−1) whereas in other months, e.g., July or August, the tidal cycles are more homogenous (with peak velocities ranging from 1.5 ms−1 to 1 ms−1). This can be clearly observed in Fig. 10, in which the flow velocity for P1 at the mid-depth layer is represented throughout a complete spring-neap cycle in March and July for P1 at mid-depth layer.

The significant differences in the annual power performance parameters between both plants is also reflected in important differences in the monthly power performance parameters (Figs. 7–9); the general trends of the performance of the two plants is, however, rather similar throughout the whole year. In the case of the power production, and in the case of capacity factor, the most important differences between both plants occur in December, when the production of P1 is 40% higher, whereas the smallest differences occur in July and August, about 37%.

Finally, as regards the availability factor (Fig. 8), the monthly differences between both plants are less important than in the case of electrical energy output (Fig. 7) and capacity factor (Fig. 9). For P1 and P2 they are in the ranges 0.5–0.6 and 0.4–0.5, respectively. The months with highest and lowest operation time are May and March, respectively. This also helps to explain the fact that the energy production during these months is similar, in spite of the fact that the peak velocities are higher in March.

5. Conclusions

In this work a comparison of the intra-annual performance of floating and bottom-fixed TSTs was performed through a case study in Ria de Ortigueira, and its implications for tidal stream energy exploitation were addressed for the first time. For this purpose, a 3D numerical model was implemented and applied to simulate the hydrodynamics of this estuary during a complete year, taken into account the energy extracted from the flow by the tidal farms. Two options were considered for the latter, consisting of floating or bottom-fixed TSTs, referred to as plants P1 and P2, respectively. The tidal plants were modelled by introducing a momentum sink term in the vertical layers of the model corresponding to the area occupied by the rotors of the turbines. The computed velocity series were then used to conduct a thorough power performance analysis based on three performance parameters allowing the characterisation of the operation of the plants: electric energy output, availability factor and capacity factor.

Remarkable differences in the power performance of both plants were found. Plant P1 presents higher values of the performance parameters considered; in particular, the annual electrical energy output is almost twice that of P2, and its capacity factors around 64% higher, showing that floating devices offer a better production to capital investment ratio. Regarding the availability factor, the differences are less important (15%); however, the power output of P1 is smoother, and this is an advantage that should not be disregarded – not least if an energy storage system is to be installed. In addition, it emerged from the intra-annual analysis that the aforementioned parameters also present a significant monthly variability. Their intra-annual general trend is similar for both plants, i.e., the annual differences are roughly maintained throughout the whole year. A finding of special interest is that, contrary to what might be expected, the months with largest peak flow velocities are not those with the highest values of the power performance parameters, including energy output.

In sum, the power performance of floating and bottom fixed TSTs at the same location can differ greatly depending on the characteristics of the hydrodynamic conditions of the coastal area in which they operate. This can be exacerbated in the case of coastal bodies with significant differences in the current velocities throughout the water column, as is the case of the study area (Ria de Ortigueira). As a result of the higher velocities near the surface, floating TSTs provide a much better performance than bottom-fixed devices. Finally, a significant intra-annual variability in the power performance was observed, which leads to the conclusion that the energy output and performance of a tidal stream farm must be analysed based on simulations covering a complete year, rather than by extrapolating the results obtained for one spring-neap cycle, as it is done following the common procedure.

Beyond the interest of these results for the coastal area herein studied, the procedure presented in this work could be used to analyse the annual power performance of different tidal stream plants elsewhere. Furthermore, in addition to the performance, which is of undoubtedly importance in the decision-making regarding the installation of a tidal stream plant, other factors such as the impact on the hydrodynamics or the long term coastal morphology should be considered before selecting the optimum farm configuration. These aspects will be dealt with as a continuation of this line of research.

Acknowledgements

This work was supported in part by project DPI2009-14546-C02-02 (“Assessment of Renewable Energy Resources”) of Spain's Ministry of Science, and in part by the project “Marine Energies” (USC 2012-PP011). During this work M. Sanchez and V. Ramos have been supported by the I2C grants PRE/2011/236 (Plan Galego de Investigación Innovación e Crecemento 2011–2015) of Xunta de Galicia.

Nomenclature

Roman

A_t	cross-sectional area of turbine rotor [m^2]
A_f	availability factor

c salinity or temperature (transported substance)
C_T thrust coefficient
C_f capacity factor
C_p power coefficient
C_{pNO} power coefficient in normal operation (Evopod turbine)
C_{pSC} power coefficient in stall control (Evopod turbine)
C_{2D} 2D-Chézy coefficient
C_{3D} 3D-Chézy coefficient
C_d wind drag coefficient
d local water depth [m]
D rotor diameter (Evopod turbine)
D_h horizontal eddy diffusivity [$m^2\ s^{-1}$]
D_v vertical eddy diffusivity [$m^2\ s^{-1}$]
E_e electrical energy output [W h]
E_e^a annual electrical energy output [W h]
f Coriolis parameter
FLH equivalent full load hours
F_x x component of the flow retarding force per unit volume [N]
F_y y component of the flow retarding force per unit volume [N]
g gravitational acceleration [$m\ s^{-2}$]
H total water depth [m]
M_x x component of the momentum generated by an external force [N m]
M_y y component of the momentum generated by an external force [N m]
n Manning coefficient
P_e electrical power output [W]
P_r rated electrical power output [W]
Q intensity of mass sources per unit area [$m^2\ s^{-1}$]
R_s source term per unit area
R_ζ correlation coefficient between computed and measured time series of sea level
R_M correlation coefficient between computed and measured time series of flow velocity magnitude
R_D correlation coefficient between computed and measured time series of flow direction
T_a reference period of time [h]
T_g period of time with the tidal plant operating [h]
u eastward component of the flow velocity [$m\ s^{-1}$]
U component of the effective flow velocity perpendicular to the turbine [$m\ s^{-1}$]
$\overrightarrow{U_{10}}$ wind velocity at 10 m height above the sea surface [$m\ s^{-1}$]
$\overrightarrow{u_b}$ horizontal velocity in the bottom layer [$m\ s^{-1}$]
V_c volume of control [m^3]
V_{ci} cut-in velocity (Evopod turbine) [$m\ s^{-1}$]
V_{co} cut-off velocity (Evopod turbine) [$m\ s^{-1}$]
V_r rated velocity (Evopod turbine) [$m\ s^{-1}$]
v northward component of the flow velocity [$m\ s^{-1}$]
w vertical component of the flow velocity [$m\ s^{-1}$]
x east direction
y north direction
z vertical direction

Greek

Δh maximum tidal range [m]
Δz_b vertical distance from the seabed to the computational grid [m]
κ von Karman constant
ζ water level [m]
λ_d first-order decay process
ρ_0 water reference density [$kg\ m^{-3}$]
ρ seawater density [$kg\ m^{-3}$]
ρ_a air density [$kg\ m^{-3}$]
$\overrightarrow{\tau_s}$ wind stress on the sea surface [$N\ m^{-2}$]
$\overrightarrow{\tau_{b3D}}$ shear stress at the bottom [$N\ m^{-2}$]
υ_h horizontal eddy viscosity [$m^2\ s^{-1}$]
υ_v vertical eddy viscosity [$m^2\ s^{-1}$]

References

[1] World Commission on Environment and Development (WCED). Our common future. 1987.
[2] European Commission. Proposal for a directive amending Directive 98/70/EC relating to the quality of petrol and diesel fuels and amending Council Directive 93/12/EC and amending Directive 2009/28/EC on the promotion of the use of energy from renewable sources [COM(2012) 595]. 2012.
[3] Bahaj AS. Generating electricity from the oceans. Renew Sustain Energy Rev 2011;15(7):3399–416.
[4] Blunden LS, Bahaj AS. Initial evaluation of tidal stream energy resources at Portland Bill, UK. Renew Energy 2006;31(2):121–32.
[5] Carballo R, Iglesias G, Castro A. Numerical model evaluation of tidal stream energy resources in the Ría de Muros (NW Spain). Renew Energy 2009;34(6):1517–24.
[6] Charlier RH. A "sleeper" awakes: tidal current power. Renew Sustain Energy Rev 2003;7(6):515–29.
[7] Neill SP, Litt EJ, Couch SJ, Davies AG. The impact of tidal stream turbines on large-scale sediment dynamics. Renew Energy 2009;34(12):2803–12.
[8] Fallon D, Hartnett M, Olbert A, Nash S. The effects of array configuration on the hydro-environmental impacts of tidal turbines. Renew Energy 2014;64(0):10–25.
[9] Hammar L, Ehnberg J, Mavume A, Cuamba BC, Molander S. Renewable ocean energy in the Western Indian Ocean. Renew Sustain Energy Rev 2012;16(7):4938–50.
[10] Khan MJ, Bhuyan G, Iqbal MT, Quaicoe JE. Hydrokinetic energy conversion systems and assessment of horizontal and vertical axis turbines for river and tidal applications: a technology status review. Appl Energy 2009;86(10):1823–35.
[11] Sanchez M, Carballo R, Ramos V, Iglesias G. Floating vs. bottom-fixed turbines for tidal stream energy: a comparative impact assessment. Energy 2014;72(0):691–701.
[12] Carballo R, Iglesias G, Castro A. Residual circulation in the Ria de Muros (NW Spain): a 3D numerical model study. J Mar Syst 2009;75(1–2):130.
[13] Iglesias G, Carballo R. Effects of high winds on the circulation of the using a mixed open boundary condition: the Ría de Muros, Spain. Environ Model Softw 2010;25(4):455–66.
[14] Iglesias G, Carballo R. Can the seasonality of a small river affect a large tide-dominated estuary? the case of the Ria de Viveiro, Spain. J Coast Res 2011;27(6):1170–82.
[15] Iglesias G, Sánchez M, Carballo R, Fernández H. The TSE index – a new tool for selecting tidal stream sites in depth-limited regions. Renew Energy 2012;48(0):350–7.
[16] Bolle A, Bing Wang Z, Amos C, De Ronde J. The influence of changes in tidal asymmetry on residual sediment transport in the Western Scheldt. Cont Shelf Res 2010;30(8):871–82.
[17] Hu K, Ding P, Wang Z, Yang SA. 2D/3D hydrodynamic and sediment transport model for the Yangtze Estuary, China. J Mar Syst 2009;77(1–2):114–36.
[18] Ramos V, Carballo R, Álvarez M, Sánchez M, Iglesias G. Assessment of the impacts of tidal stream energy through high-resolution numerical modeling. Energy 1 November 2013;61:541–54.
[19] Ramos V, Carballo R, Álvarez M, Sánchez M, Iglesias G. A port towards energy self-sufficiency using tidal stream power. Energy 2014;71(0):432–44.
[20] Iglesias G, Carballo R. Seasonality of the circulation in the Ría de Muros (NW Spain). J Mar Syst 2009;78(1):94–108.
[21] Sánchez M, Carballo R, Ramos V, Iglesias G. Tidal stream energy impact on the transient and residual flow in an estuary: a 3D analysis. Appl Energy 2014;116(0):167–77.
[22] Ramos V, Carballo R, Sanchez M, Veigas M, Iglesias G. Tidal stream energy impacts on estuarine circulation. Energy Convers Manag 2014;80(0):137–49.
[23] User manual Delft3D-WAVE. Delft, The Netherlands: Deltares ed; 2010.
[24] Dyer KE. Estuaries: a physical introduction. New York: John Wiley; 1997.
[25] Defne Z, Haas KA, Fritz HM. Numerical modeling of tidal currents and the effects of power extraction on estuarine hydrodynamics along the Georgia coast, USA. Renew Energy 2011;36(12):3461–71.
[26] Ahmadian R, Falconer RA. Assessment of array shape of tidal stream turbines on hydro-environmental impacts and power output. Renew Energy 2012;44(0):318–27.
[27] Ahmadian R, Falconer R, Bockelmann-Evans B. Far-field modelling of the hydro-environmental impact of tidal stream turbines. Renew Energy 2012;38(1):107–16.
[28] Bahaj AS, Molland AF, Chaplin JR, Batten WMJ. Power and thrust measurements of marine current turbines under various hydrodynamic flow conditions in a cavitation tunnel and a towing tank. Renew Energy 2007;32(3):407–26.

Please cite this article in press as: Sánchez M, et al., Energy production from tidal currents in an estuary: A comparative study of floating and bottom-fixed turbines, Energy (2014), http://dx.doi.org/10.1016/j.energy.2014.09.053

[29] Ramos V, Iglesias G. Performance assessment of tidal stream turbines: a parametric approach. Energy Convers Manag 2013;69(0):49–57.
[30] Bahaj AS, Myers L. Analytical estimates of the energy yield potential from the Alderney Race (Channel Islands) using marine current energy converters. Renew Energy 2004;29(12):1931–45.
[31] Evans G, Prego R. Rias, estuaries and incised valleys: is a ria an estuary? Mar Geol 2003;196(3–4):171–5.
[32] Dyer KR. Estuaries: a physical introduction. London: John Wiley & Sons; 1973.
[33] Perillo GME. Chapter 2 Definitions and geomorphologic classifications of estuaries. Developments in sedimentology: Elsevier, 17–47.
[34] Mendez G, Rey D. An historical review of the geological studies of the Galician rias. J Iber Geol 2000;26:21–44.
[35] Sánchez M, Iglesias G, Carballo R, Fraguela JA. Power peaks against installed capacity in tidal stream energy. IET Renew Power Gener 2013;7(6):246–53.
[36] Oceanflowenergy. www.oceanflowenergy.com [accessed 10.07.14].
[37] Philips NA. A co-ordinate system having some special advantages for numerical forecasting. J Meteorol 1957;14:184–5.
[38] Rodi W. Examples of calculation methods for flow and mixing in stratified fluids. J Geophys Res 1987;92(C5):5305–28.
[39] Cheng RT, Casulli V, Gartner JW. Tidal, Residual, Intertidal Mudflat (TRIM) model and its applications to San Francisco Bay, California. Estuar Coast Shelf Sci 1993;36(3):235–80.
[40] Dias JM, Sousa MC, Bertin X, Fortunato AB, Oliveira A. Numerical modeling of the impact of the Ancão inlet relocation (Ria Formosa, Portugal). Environ Model Softw, In Press, Corrected proof.
[41] Dias JM, Lopes JF. Implementation and assessment of hydrodynamic, salt and heat transport models: the case of Ria de Aveiro Lagoon (Portugal). Environ Model Softw 2006;21(1):1–15.
[42] Smith SD. Wind stress and heat flux over the ocean in gale force winds. J Phys Oceanogr 5, May 1980;1980(10):709–26.
[43] Yelland MJ, Moat BI, Taylor PK, Pascal RW, Hutchings J, Cornell VC. Wind stress measurements from the open ocean corrected for airflow distortion by the ship. J Phys Oceanogr 1998;28(7):1511–26.

Please cite this article in press as: Sánchez M, et al., Energy production from tidal currents in an estuary: A comparative study of floating and bottom-fixed turbines, Energy (2014), http://dx.doi.org/10.1016/j.energy.2014.09.053